Bioelectrochemistry 138 (2021) 107734

Contents lists available at ScienceDirect

Bioelectrochemistry

journal homepage: www.elsevier.com/locate/bioelechem

A nano-composite based regenerative neuro biosensor sensitive to Parkinsonism-associated protein DJ-1/Park7 in cerebrospinal fluid and saliva

Münteha Nur Sonuç Karaboğa [a,*], Mustafa Kemal Sezgintürk [b]

[a] Tekirdağ Namık Kemal University, School of Health, 59030 Tekirdağ, Turkey
[b] Canakkale Onsekiz Mart University, Faculty of Engineering, Bioengineering, Canakkale, Turkey

ARTICLE INFO

Article history:
Received 15 September 2020
Received in revised form 22 December 2020
Accepted 23 December 2020
Available online 29 December 2020

Keywords:
Parkinson's disease
Neurodegeneration
Biosensor
MWCNT
DJ-1

ABSTRACT

In this study, we developed an electrochemical-based single-use neurobiosensor based on multiwalled carbon nanotube (MWCNT)-gold nanoparticle (AuNP) nanocomposite doped, 11-amino-1-undecanethiol (11-AUT)-modified polyethylene terephthalate coated indium tin oxide (ITO-PET) electrodes. This electrode was used for the sensitive determination of DJ-1, a protein responsible for mitochondrial dysfunction in Parkinson's disease (PD) with the task of eliminating oxidative stress.

The design strategy and analytical studies for the neurobiosensor were monitored with electrochemical impedance spectroscopy (EIS), cyclic voltammetry (CV) and single frequency impedance (SFI) techniques. The selective determination range for DJ-1 of the developed neurobiosensor system is 4.7–4700 fg mL^{-1} in accordance with the charge transfer resistance (Rct) associated with a limit of detection of 0.5 fg mL^{-1}.

Since changes in the expression of DJ-1 protein is particularly important in cerebrospinal fluid (CSF) and saliva, the ability of the developed neurobiosensor system to detect the DJ-1 protein in these media was tested by the standard addition method. The statistical results show that the biosensor decorated with MWCNT-AuNP-AUT may be recommended for the selective determination of DJ-1 protein.

1. Introduction

DJ-1 (also called PARK-7 or Parkinsonism associated deglycase) is the gene responsible for the genetic form of Parkinson's disease (PD) and plays an important role in antioxidant defenses to protect cells from oxidative stress [1,2]. DJ-1 is a homodimeric protein of 189 amino acids [3,4] and is mainly expressed in the glial cells in the cortex and in the neurons of the substantia nigra and striatum [5]. Studies have shown that the loss of function of the DJ-1 protein is one of the causes of Parkinson's disease, but that it is used in the treatment of cancer. This can be explained by the role DJ-1 plays in oxidative stress being a common denominator [4]. Many studies have shown that mutations in DJ-1 are associated with autosomal recessive early-onset PD [5,6] and it is likely to be associated with mitochondrial dysfunction as it is an important protein involved in the elimination of oxidative stress [7]. Recent studies suggest that DJ-1 protein is closely related to PD, and that DJ-1, which is present in both cerebrospinal fluid [6,8,9] and saliva [10–13] with concentration varying in the event of disease, may also be a potential marker.

Diagnosis of PD is usually based on clinical history and motor symptoms. When motor symptoms occur, more than half of the dopaminergic neurons in the substantia nigra pars compacta are thought to be lost and the disease is in the middle or late stage [14]. It is clear, however, that the neurodegeneration of the disease began decades previously [15]. Therefore, the importance of early diagnosis for PD is very urgent and it is thought that increasing the accuracy for diagnosis of PD will help to differentiate the disease from other forms of parkinsonism [16,17].

Carbon nanotubes (CNTs) are nanostructured carbon allotropes that can have a diameter/length ratio greater than 1,000,000. This magnificent strength of carbon nanotubes from the derives of sp2 carbon–carbon bonds in the structure. This popularity and usefulness of CNTs is thanks to its mechanical, thermal and electronic properties. CNTs are one of the most powerful materials ever discovered by humanity [18,19]. Successful integration of MWCNT in biological detection applications is accompanying high surface area with high conductivity and result of electron transfer with biocompatibility. [19,20]. AuNPs, another material commonly used in the field of biosensing, are indispensable for their inert structure,

* Corresponding author.
E-mail address: mnsonuc@nku.edu.tr (M.N. Sonuç Karaboğa).

https://doi.org/10.1016/j.bioelechem.2020.107734
1567-5394/

biological compatibility and easy modification for the target analyte such as peptides, proteins and aptamers to specifically recognize biological targets [21]. Gold nanoparticles are used with very different strategies in electrochemical-based biosensors. For example, in a study for the determination of bovine leukemia virus antigen gp51, antibodies modified with magnetic gold nanoparticles were used as biorecognition elements. The sensitivity of the method is enhanced using Raman tags, which consist of gold nanorodes coated with a layer of 5-thio-nitrobenzoic acid with covalently linked antibodies. The researchers emphasized that the role of the use of magnetic gold nanoparticles in the rapid, reliable and selective immunological test they developed is undeniable [22].

EIS is an electrochemical technique that is used especially frequently in the design of immuno-interaction-based biosensors and determination of binding events on the transducer surface and has many superior features. An advantage of EIS based biosensor is its simple preparation, fast response, low cost, negligible effect on changing environmental conditions and the opportunity of applying different types of analytes such as proteins, nucleic acids, cells, microorganisms, antibodies and antigens [23–26]. The process is noninvasive, sensitive and, therefore, very suitable for the patient. EIS has limited disadvantages. One of them is the EIS instrument being expensive [27,28]. In addition, the three basic requirements for AC impedance measurements, linearity, stability and causality, must be obtained. The accuracy of the EIS measurement depends not only on the technical precision of the instrumentation but also on the operating procedures [24]. However, there are relatively few limitations that arise due to the design of the biosensor. For example, if the sensing surface is too thin, decreasing the signal to noise ratio will lead to a decrease in sensitivity in EIS measurements [29,30]. In addition, small molecules such as heavy metals, pesticides, or antibiotic residues are difficult to analyze with EIS from real samples [31].

The design strategy of this neuro-biosensor for the detection of DJ-1 involves covalent bonding of MWCNT on the surface of 11-AUT-assembled AuNPs-doped ITO-based disposable electrodes. The developed neuro biosensor has high sensitivity, reproducibility, regenerative and remarkable storage capacity. The pinhole diameters of the self-assembled monolayer of 11-AUT and the Kramer's Kronig data, which allow interpretation of instrumental errors used in sensor design, were also calculated. MWCNT-AuNP-based single-use neurobiosensor can maintain and detect susceptibility to the target DJ-1 protein in both CSF and saliva media.

2. Experimental

2.1. Materials

An electrochemical triple electrode system was used throughout the study (Reference: Ag/AgCl, counter: platinum wire and working electrodes: disposable ITO-coated PET films, 2 × 0.5 cm) were obtained from BASi (West Lafayette, IN, USA) and Sigma Aldrich (St Louis, MO, USA). DJ-1 from human plasma and monoclonal anti-DJ-1 (anti-PARK7) antibody from rabbit were obtained from Sigma Aldrich (St Louis, MO, USA). Antibody and antigen were maintained at −20 °C in portions prepared in pH 7.0 phosphate buffer throughout the study. EDC-NHS couple, MWCNT and Au (III) chloride trihydrate were also supplied by Sigma Aldrich (St Louis, MO, USA). FTIR spectra, operating in the range of 4000–400 cm^{-1}, were recorded. Morphological changes in nanocomposites and immobilization steps were monitored by SEM (FEI-Quanta FEG 250 Model) and AFM. AFM analysis was performed at NKÜ Scientific and Technological Research Center (NABILTEM) using AFM PLUS +, NanoMagnetic Instruments. Images were obtained using the AFM tapping mode (256 × 256 points with scan rate 5 μm/s.).

2.2. Preparation of sensing surface and functionalization of gold nanoparticles

Before proceeding to the advanced design steps of the neuro-biosensor, the ITO-PET disposable electrodes are cleaned as described in our previous studies in detail [32,33]. The sensing unit formed on the surface of active -OH groups was washed with ultra-pure water and dried with argon gas respectively, then immersed in an electrochemical cell containing $HAuCl_4{\cdot}3H_2O$ (1 mM) solution in 50 mM pH 7.0 phosphate buffer. Electrochemical deposition of gold nanoparticles on the ITO sensing surface was performed in 10 consecutive cycles at a scanning rate of 50 mV/s between −0.2 V and (−)1.3 V [34]. Gold nanoparticle-doped ITO electrodes were immersed in a solution of 11-AUT prepared in ethanol solution to form SAMs on the surface and allowed to incubate overnight. After incubation, the electrodes were washed with ethanol to remove unbound amino thiols.

2.3. Decoration of DJ-1 neuro-biosensor

The MWCNT-COOH materials were dispersed in 0.1 mol/L Sodium dodecyl sulfate (SDS) solution (30 min with sonication) [35] before immobilization of the carbon nanotube to the sensing unit surface. The MWCNT-COOH was then activated for 45 min with a solution of 1 mM NHS and 4 mM EDC prepared in phosphate buffer to convert the terminal carboxylic groups present in the structure to an active NHS ester. Subsequently, the activated MWCNTs were incubated with amino-thiol-functionalized gold nanoparticle-doped ITO electrodes to generate the nano-composite for 2 h [36]. The prepared nano-composite active sensors were washed with ultra-pure water, dried with ultra-pure argon gas and then immersed in solution containing 100 μL of anti-DJ-1 antibody and allowed to incubate for 60 min at room temperature in the dark. After immobilization with anti-DJ-1 antibody, the washing step was repeated to remove unbound groups and the sensing unit was dried with argon gas. Finally, the electrodes immobilized with DJ-1 were incubated for 60 min in 0.5% BSA solution to block non-reactive ends and prevent non-specific interactions. With this last step, the prepared neuro-biosensor was stored at +4 °C until DJ-1 measurements were performed. Bare and modified ITO surfaces are expressed as ITO, ITO-OH, ITO-OH/AuNP, ITO/OH/AuNP /11-AUT, ITO/OH/AuNP /11-AUT/MWCNT, ITO/OH/AuNP/11-AUT/MWCNT/anti-DJ-1, ITO/OH/AuNP/11-AUT/MWCNT/anti-DJ-1/BSA, and ITO/OH/AuNP/11-AUT/MWCNT/anti-DJ-1/BSA/DJ-1. The design strategy of the biosensor is schematized in Scheme 1.

2.4. Electrochemical biosensor measurements

The neuro-biosensor decorated with MWCNT-AuNP was read using the commercial Gamry Potentiostate/Galvanostate, Interface 1000 system (Gamry Instruments, Warminster, USA) including CV and EIS software previously described in detail [37]. All electrochemical experiments were performed in solution containing 5 mM K_3 [Fe (CN) $_6$]/K_4 [Fe (CN) $_6$] (1:1) as the redox probe. The redox probe solution contains 0.1 M KCl to reduce the resistance of the probe solution. The EIS parameters are as follows: the direct current potential was 0.2 V, the frequency range was from 0.5 Hz to 500,000 Hz. EIS analysis was carried out by applying an alternating potential of 5 mV and the formal potential was 0 V.

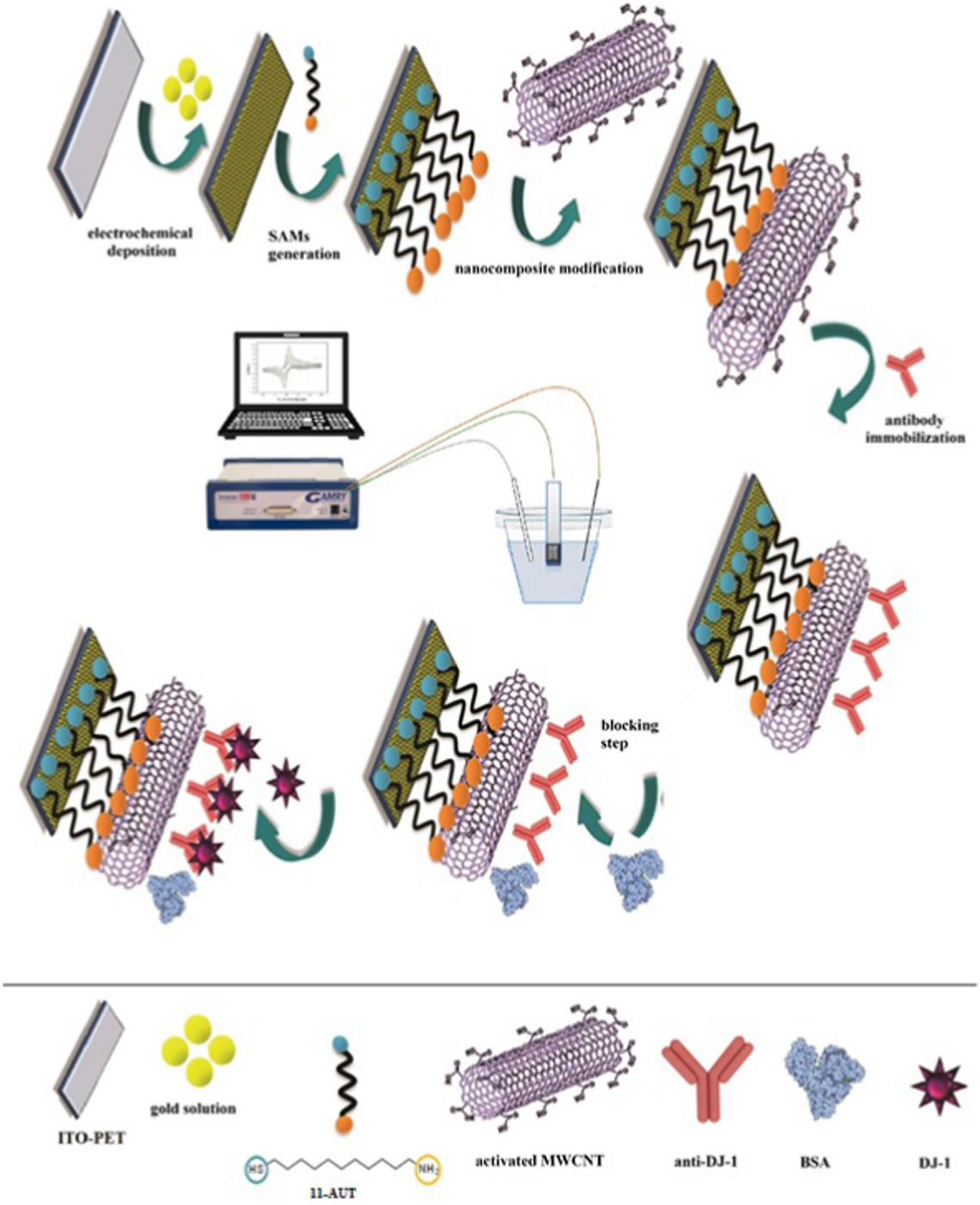

Scheme 1. Schematic presentations of neuro-biosensor.

2.5. Analysis of protein DJ-1 with the constructed neuro-biosensor system

Each of the 11-AUT-modified, MWCNT-AuNP-doped ITO-based neuro-biosensing electrodes was incubated with standard DJ-1 solutions prepared at different concentrations for 60 min at room temperature and in the dark. After the incubation period, the neurobiosensor was washed with ultra-pure water to remove physically adsorbed DJ-1 molecules. EIS and CV measurements of each DJ-1 concentration were performed by measuring at the working electrodes on the redox probe. EIS and CV measurements were evaluated by EChem Analyst software.

2.6. CSF and saliva samples test

The behavior of the developed neurobiosensor in complex media was monitored by analyzing the DJ-1 concentration with the standard addition method in human cerebrospinal fluid and saliva samples. The DJ-1 concentrations used for standard addition were selected from the points on the standard plot, 235 fg mL^{-1} and 3500 fg mL^{-1}. Measurements were repeated 3 times for each CSF and saliva sample. Samples were collected randomly from Namık Kemal University Medical School Hospital with the approval of the ethics committee numbered 2013/86/07/05. CSF samples were collected and stored at −20 °C in certain portions

until measurements were performed; saliva samples were stored at +4 °C.

3. Results and discussion

3.1. Electrochemical evidence of constructed neuro-biosensor

AuNPs and MWCNT are the basis of the nanocomposite structure within this neuro-biosensor system developed for sensitive capture of target protein DJ-1, a biomarker candidate for the evaluation of PD. AuNPs are capable of transferring electrons between the electroactive biological species and the electrode. The multi-walled carbon nanotube has advanced capacities to approach the active site of the biosensing unit and connect it to the electrode. Furthermore, its ease of functionalization provides new features for nanostructured electrodes such as specific sites for biomolecules or redox mediation of bioelectrochemical reactions [38]. The proximity of the MWCNT to the redox center enables fast and efficient electron transfer. The driving force in immobilization of anti-DJ-1 on the sensing unit modified with MWCNT is hydrophobic interactions. In this proposed neuro-biosensor system for the determination of DJ-1, the SAMs layer (with 11-AUT) exhibits excellent packaging properties in molecular order; the conductivity of the gold nanoparticle benefits its role as a redox mediator; and MWCNT has a high surface-to-volume ratio, making it possible to detect DJ-1 very quickly, even at low concentrations.

Fig. 1A clearly shows the cyclic voltammograms recorded during the electrochemical synthesis of Au nanoparticles by electrochemical deposition on the ITO surface.

Initially (in the first cycle), the reduction of Au occurred at about −935 mV against the Ag/AgCl reference electrode, but with repeated screening cycles the reduction potential shifted to −1.005 V in the final cycle, depending on the nucleation of the deposition (graph inserted in Fig. 1A). This shift is proof that the gold nanoparticle was successfully deposited on the sensing surface.

After electrochemical deposition of gold nanoparticles on the ITO-PET surface, the SAM layer was formed on the surface with 11-aminoundecanetiol. Covalent interaction between Au and SH functional group was achieved by overnight incubation. The electrodes were then treated with EDC-NHS-activated–MWCNT to form functional –COO groups on the surface. After anti-DJ-1 antibody was immobilized to the MWCNT-modified surface, BSA was used to terminate active terminal ends and avoid non-specific binding. The impedance spectra taken from EIS of the steps during the construction of the neuro-biosensor developed for the determination of DJ-1, the charge transfer changes at each step and the voltammograms taken from CV are shown in Fig. 1.

This equivalent circuit model (Fig. 1C), which is frequently used in impedimetric immunosensor studies, consists of resistance and capacitive elements as well as the Warburg element. Rct is the charge transfer resistance, Rst indicates the resistance of the working solution of the system, CPE is the stationary phase element of the bioactive layer, and Zw is the Warburg element. The most striking change among these elements belongs to the charge transfer resistance (Rct). This circuit has been applied to describe the flow of electron transfer from electrolyte to electrode. It has been reported that different EIS circuit models were used in studies where different surface modifications were applied [39]. The applied circuit model provides valuable information about the electrical model of the sensing system.

The high insulating properties of the ITO-PET electrodes do not permit electron transfer, which leads to high charge transfer resistance (approximately 40 kΩ). The electrochemical deposition of gold nanoparticles on the sensing surface provides the electrodes effective conductive behavior, resulting in reduced charge transfer resistance (approximately 100 Ωs). Compared to bulk gold surfaces, gold nanoparticles have a higher surface area; it allows a larger amount of protein to load and is potentially more sensitive.

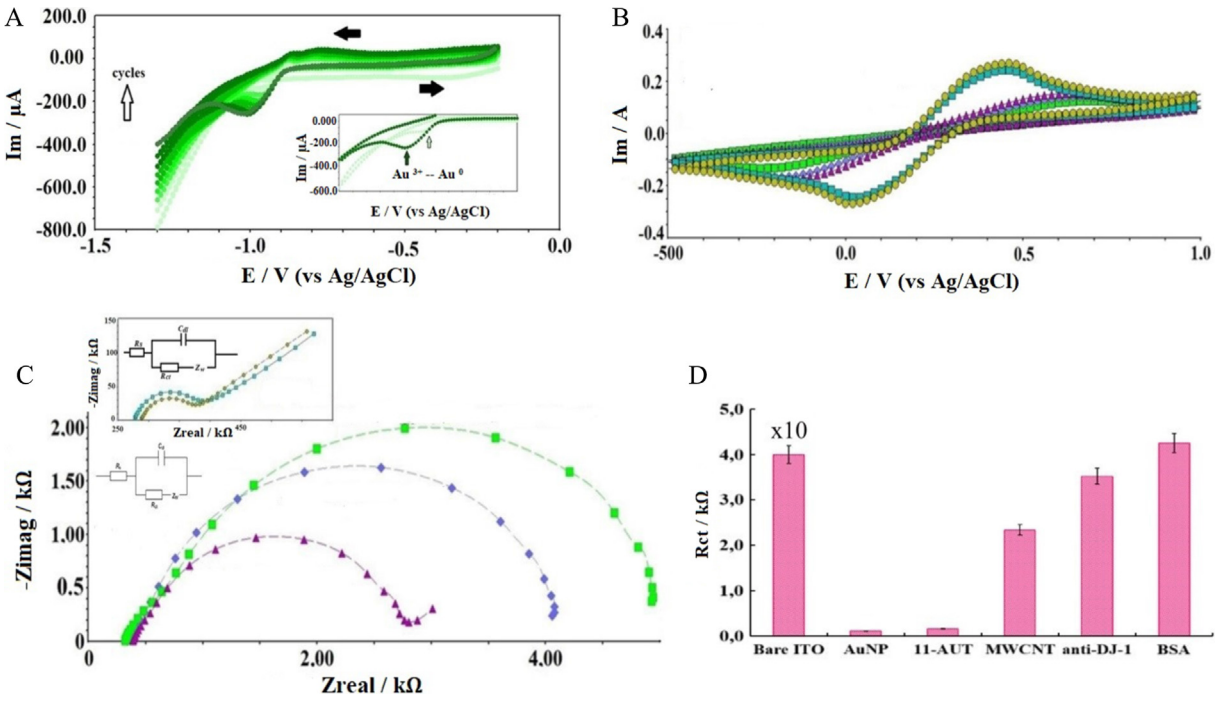

Fig. 1. Cyclic voltammograms of the gold nanoparticle depositing on the ITO electrode surface (A), cyclic voltammograms (B), Electrochemical impedance spectra (C), [-●-●-: ITO/AuNP, -■-■▲-: ITO/AuNP /11-AUT, -▲-▲-: ITO/AuNP /11-AUT/MWCNT, -◆-◆-: ITO/AuNP/11-AUT/MWCNT/anti-DJ-1, and green -■-■-: ITO/OH/AuNP/11-AUT/MWCNT/anti-DJ-1/BSA and charge transfer changes (D) for immobilization steps. (For interpretation of the references to color in this figure legend, the reader is referred to the web version of this article.)

Compared to bulk, especially the thiol-modified gold nanoparticle has superior eelectronic properties in recognizing the biological material and creating a biorecognition unit. [40]. The charge transfer resistance of gold nanoparticle-coated ITO electrodes increased slightly after treatment with 11-AUT (Fig. 2C–D). The interaction between sulfur and gold is thought to continue by oxidative addition of the thiol (-SH) group to the metallic gold surface followed by reduction of hydrogen. The increase in SAM formation depends on the number of CH_2 units in the structure [41]. The terminal positive amino groups in the 11-AUT, which contribute to altering the surface properties of the sensing unit, attract the negative redox probe, making the diffusion of electrons to the surface possible, and resulting in almost no change to charge transfer resistance relative to the gold nanoparticle deposition step (Fig. 1C–D). The 11-AUT-modified electrodes were treated with MWCNT with carboxylate groups activated with EDC-NHS. The amino terminal groups in the 11-AUT and some of the active –COO groups with MWCNT form the amide bond, while the non-bonding active –COO groups partially complicate the diffusion of the redox probe to the surface, causing an increase in charge transfer resistance. The large p-conjugated system in MWCNTs allows the structure to act as electron acceptor and donor. After the ITO-based electrodes were modified as described above, a biorecognition unit was established with immobilization of anti-DJ-1. The amide bond between the active –COO groups and $–NH_2$ accompanied good packing on the surface, making transfer of electrons difficult. As can be seen from the impedance spectrum (Fig. 1C), this result supports the successful immobilization of anti-DJ-1 onto the hybrid surface. The intention is to avoid functional terminals and non-specific binding by treatment with BSA, which once again increases the charge transfer resistance due to the protein barrier formed.

The heterogeneous electron transfer rate constant value (k0) of the redox probe is an important factor used to verify the electronic transport process in the nanocomposite film. The k0 value of the production steps of the neuro-biosensor are calculated (detailed description of the equation is provided in the supplemental data). As can be seen in Table 1, deposition of gold nanoparticles on the ITO sensing surface followed by the formation of SAMs by 11-AUT showed a high k0 value, which is a result of increased electron transport. The immobilization of anti-DJ-1 antibody then shows a significant decrease in the k0 value (6.0×10^{-9} m.s^{-1}). It confirms the slow electron transport and formation of the biosensing unit due to the isolating property of protein molecules.

Progressive steps in the neuro-biosensor system, consisting of AuNP, 11-AUT and MWCNT, and ultimately immobilization of the anti- DJ-1 onto the sensing surface, increase the thickness of the double loaded layer and inhibit the interface electrochemical process of the redox probe. Electrode capacitance and double layer capacitance (Cdl) decrease while electron transfer resistance increases and Rct respectively. This is the result of the impedimetric behavior of the developed neuro-biosensor system.

When developing the neuro-biosensor system for the detection of DJ-1, the peak potential separation between anodic and cathodic waves (△Ep) was calculated. Accordingly, when the ITO electrodes were coated with gold nanoparticle at a scanning rate of 100 mV/s and subsequently modified with 11-AUT the △Ep value was calculated to be 0.43 V, and after the MWCNT modification the △Ep value increased to 0.78 V. This increase is proof that the MWCNT

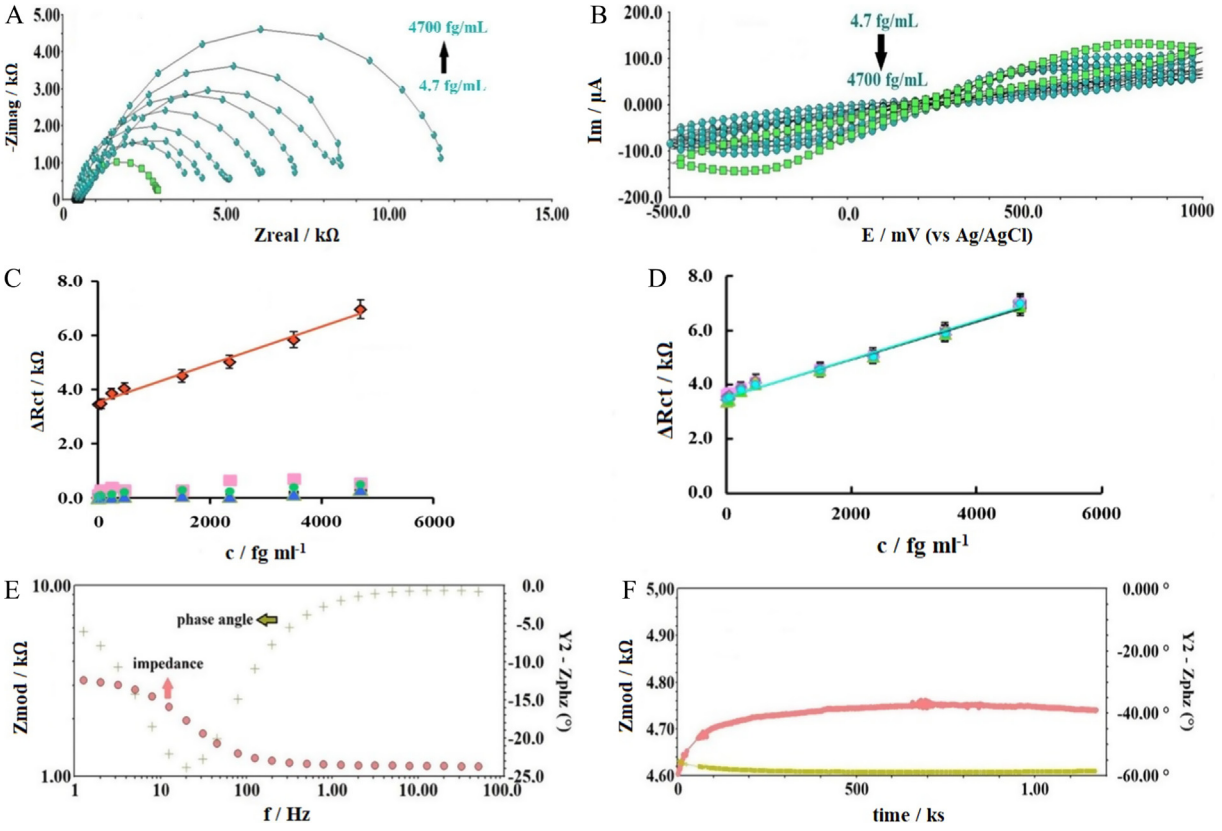

Fig. 2. Impedance spectra (A), cyclic voltammograms (B) obtained for different concentrations of DJ-1 [-■-■-: ITO/BSA, and -●-●-: ITO/DJ-1] concentration-dependent calibration curve for -◆-◆-: DJ-1 [y = 0.6973x + 3528.2, R^2: 0.9867], -■-■-: SYN-alpha, -▲-▲-: HSP-70, -●-●-: Tau-441 obtained using the neuro-biosensor based on anti-DJ-1 under optimal working conditions (C), reproducible EIS Signal of optimized neuro-biosensing unit (D), Bode plot (E) and SFI spectrum [-●-●-: impedance, -■-■-: phase angle] (F) of the designed neuro-biosensor.

Table 1
Impedimetric parameters of neuro-biosensor design steps.

Neuro-biosensor	**Ru**/Ω	**C_{dl}**/μF	**k^0/m.s^{-1}**	**K.K.T**/μ
ITO/AuNP	308.7 ± 2.2	12.12 ± 0.9	2.11×10^{-8}	6.8
ITO/AuNP/11-AUT	293.6 ± 2.3	4.05 ± 0.3	1.34×10^{-7}	1.1
ITO/AuNP/11-AUT/MWCNT	416.9 ± 2.9	3.42 ± 0.05	9.1×10^{-9}	4.1
ITO/AuNP/11-AUT/MWCNT/anti-DJ-1	374.2 ± 2.6	3.05 ± 0.05	6.0×10^{-9}	9.8
ITO/AuNP/11-AUT/MWCNT/anti-DJ-1/BSA	358 ± 2.4	2.58 ± 0.06	5.0×10^{-9}	50.7

layer greatly reduces conductivity due to the active carboxylic terminals. After the immobilization of anti-DJ-1, the △Ep value increased to 0.88 V, supporting the CV results showing that the immobilization was performed successfully (Fig. 1B).

Impedance data are useful tools for determining the surface coverage (θeis) and other kinetic parameters of monolayer electrodes. After the ITO electrodes had gold nanoparticles deposited electrochemically on the surface, forming SAMs with 11-AUT, the surface coverage value and pinhole results were calculated by using EIS data (the equations given in supplemental data). Accordingly, after SAMs was formed with 11-AUT, the θeis value was 0.9946. The radius of the pinhole was found to be 1.63 μm and the distance between the two pinholes was calculated as 22.18 μm. With these values, it can be concluded that 11-AUT covers the sensing surface very well and contains minimum defects. Regular and minimum defect packing on the surface can be explained by the strength of the bond between Au-S and the excess $-CH_2$ groups found in 11-AUT stabilizing the structure. It was reported that as the number of carbons in the alcaetiols is reduced, the defect and pinholes increase and the surface coating ratio decreases [42].

3.2. Optimization studies of the neuro-sensing construction parameters

The path to a well-organized immobilization process passes through the chemical affinity of 11-AUT molecules. The ideal detection matrix consists of receptor molecules supported in an inert matrix that directs and positions them to minimize kinetic and steric constraints. In a system with many kinetic and steric barriers, non-specific interactions are possible. The first step to avoid this is to optimize the 11-AUT concentration. For this purpose, AuNP-deposited ITO electrodes were incubated with 11-AUT (1, 5, 10, 50 mM) at different concentrations overnight at room temperature. Different AUT concentrations exhibited different impedimetric behaviors, since the stacking of the surface layer was greatly influenced by the concentration. As shown in Fig. 1S (supplemental data), the neuro-biosensor system prepared with 50 mM 11-AUT has a relatively high charge transfer resistance and a relatively low detection coefficient on the regression curve, while the biosensor prepared with 1 mM 11-AUT has a low charge transfer resistance and a relatively high detection coefficient (R^2: 0.6788). As can be seen from the calibration graph, hydrophobic interactions caused by the increased concentration of 11-AUT, as well as the excessively increased aliphatic chain, prevent successful immobilization of anti-DJ-1 and increase charge transfer by causing non-specific binding. However, 5 mM 11-AUT has a relatively high charge transfer resistance and a high detection coefficient (R^2: 0.9709), and further steps were performed with this optimized value.

Superior to conventional solid electrodes, biosensor systems using MWCNT appear to have high sensitivity, fast response times, and the ability to detect target analyte in wide detection ranges [43]. The difference in surface microenvironment results in a different distribution of surface energy for the MWCNTs, which can provide a plurality of active sites so that the functionalized MWCNTs have good catalytic activity for biomolecules [44]. High surface activity has the advantage of electron transfer between anti-DJ-1 antibody and MWCNT, which is possible only when MWCNT achieves direct electronic transmission. A major problem for the preparation of MWCNTs as biosensors is the solubility of MWCNTs. In preparing this neuro-biosensor, the dissolution problem of MWCNT was overcome by dispersions prepared in aqueous SDS solution.

For the amide bond formed between the MWCNTs activated by EDC/NHS and the 11-AUT, the structure is functional. Although covalent modification can improve the properties of MWCNTs to some extent, stability is partially affected because the sp2 structure of MWCNTs is destroyed. The MWCNTs prepared at different concentrations (0.085; 0.17; 0.255 mg/mL) and the impedimetric response of the neuro-biosensor were monitored. It was found that the functional structure prepared with 0.085 mg/mL MWCNT rapidly reached saturation point after the immobilization of anti-DJ-1 in the step when DJ-1 was measured. However, similar responses were obtained from neuro-biosensors prepared with MWCNT of 0.17 mg/mL and 0.255 mg/mL (Fig. 2S). The subsequent steps were therefore continued with MWCNT prepared at a concentration of 0.17 mg/mL.

In this study, determination of the optimum concentration for the 11-AUT-generated SAMs layer and subsequent modification by MWCNT plays a key role in the successful immobilization of the anti-DJ-1 antibody. The determination of the optimal concentration for 11-AUT is also important to prevent denaturation of the biomolecule (anti-DJ-1) on the electrode surface and to increase its stability. The final step of the optimization studies is to determine the concentration of the biorecognition unit. For this purpose, neurobiosensors were prepared with different concentrations of anti-DJ-1 antibody (1, 5, 20 and 100 ng/mL) for 60 min at room temperature. It was found that the neuro-biosensor designed using 1 ng/mL anti-DJ-1 antibody concentration was insufficient for high concentration DJ-1 measurements; however, when 100 ng/mL anti-DJ-1 antibody concentration was used, the system could not give a linear response (R^2: 0.4621). Neurobiosensor systems prepared at concentrations of 5 ng/mL and 20 ng/mL had similar regression coefficients (R^2: 0.9651 and 0.9876 respectively), increasing the concentration to 20 ng/mL increased charge transfer resistance due to the efficacy of the resulting protein barrier. Thus, the anti-DJ-1 antibody concentration was optimized to 20 ng/mL for an ideal neuro-biosensor system (Fig. 3S).

3.3. Analytical performance of DJ-1 neurobiosensor

Standard DJ-1 solutions prepared at different concentrations were measured by EIS and CV techniques with a single-use neuro-biosensor system based on AuNP/11-AUT/MWCNT, the optimum conditions of which were determined. The relationship between DJ-1 concentration and electron transfer resistance was determined by the equivalent circuit model added to Fig. 1C.

It is known that a semicircle diameter obtained from the impedance curves is a measure of the charge transfer resistance (Rct). The impedance spectra obtained after adding the antigen at different concentrations are shown as Nyquist plots in Fig. 2A, where Zr

is the real part and Zim is complex, the imaginary part of impedance. At low frequencies, the impedance module clearly increases with the increase in the concentration of DJ-1, indicating that DJ-1 interacts with a larger amount of the bio-functional surface and that the resulting complex is responsible for the inhibition of electron transfer. It was observed that the relationship between increased DJ-1 concentration and charge transfer resistance reached a linear regression in the range of DJ-1 concentration of 4.7 fg mL^{-1} to 4700 fg mL^{-1} (Fig. 2C). The LOD (detection limit) and LOQ (quantification limit) values of this developed nanocomposite-modified neuro-biosensor system for DJ-1 were 0.5 fg mL^{-1} and 1.65 fg mL^{-1}, respectively. These results emphasize that the presented hybrid structure has excellent capture ability for DJ-1 antibody-antigen binding.

EIS is a very suitable technique for analyzing the electrical properties of the modified sensing probe, i.e. when an antibody immobilized on the electrode reacts with its respective antigen. This interaction allows changes in electrical properties, such as capacitance and resistance, on the electrode surface, and hence biorecognition. Table 1 shows the changes in solution resistance and double layer capacitance due to increasing DJ-1 concentration.

The reduction of the total capacitance of the system is the result of binding of the analyte to its specific receptor. The interaction of the biorecognition element with the analyte induces the change of signal in the sensor, causing the change of dielectric properties and/or conformationality [43]. Changes in Rct and capacitance with the increase in the DJ-1 concentration support the concentration-dependent formation of the antigen–antibody complex on the surface by impedimetric data. The results from the cyclic voltammograms of the DJ-1 biomarker in the concentration range of 4.7–4700 fg mL^{-1} are shown in Fig. 2B. Anodic and cathodic peak currents decreased due to increasing DJ-1 concentration. These results emphasize that electron transfer at the surface becomes difficult with increasing protein concentration. In this respect, EIS and CV results are consistent.

The values of Kramers Kronig transformations (K.K.T) for the neuro-biosensor system developed for DJ-1 determination are given in Table 1. K.K.T associate the real and imaginary components of a complex transfer function and are a powerful tool for validating EIS data. It can be used to check whether the transfer function is stable, causal or linear. However, they can only be evaluated for K.K.T under sufficient conditions. Many studies have emphasized that the Kramers - Kronig transformations are generally susceptible to breaking of causality and stability [44].

The repeatability of the ITO-based AuNP/11-AUT/MWCNT-doped neurobiosensor was determined by analyzing DJ-1 at the same concentration (470 fg mL^{-1}) with the sensor prepared with 15 disposable biosensor under similar conditions. As a result of the repeatability study, the coefficient of variation was calculated as 1.88% mean value and the standard deviation as 476.75 and 9.01 fg mL^{-1}, respectively, and it was emphasized that the developed system had very good repeatability capacity.

Unlike repeatability studies, reproducibility is the ability of the biosensor to produce the same responses for the amplified assay setup. Reproducibility is an important parameter used to characterize the accuracy of the transducer and electronics in the developed neuro-biosensor. The reproducibility of the presented nanocomposite-modified ITO-based single-use DJ-1 neuro-biosensor was evaluated by monitoring the DJ-1 responses in the concentration range of 4.7–4700 fg mL^{-1} of 6 biosensor systems prepared at different times by the same procedure. As a result of reproducibility studies, it was found that the responses of 6 neuro-biosensors showed similar linearity for DJ-1 between 4.7 and 4700 fg mL^{-1}. The relative standard deviations of the slopes and intercepts of reproducibility shown in Fig. 2D were found to be 1.73% and 2.16%, respectively. Reproducible signals have led to the assessment that the developed neurobiosensor exhibits high reliability and robustness even when conditions change on the DJ-1 responses.

Regeneration of biosensors helps reusability and increases the commercial viability of the sensors. For regeneration of the biosensors, it was observed that the solvent medium must be altered to weaken analyte/receptor binding. Regeneration studies provide an idea about the strength and sustainability of the biorecognition element of the developed biosensor. Regeneration of the developed neuro-biosensor was carried out by immersing the AuNP/11-AUT/MWCNT-modified sensor into 0.05 M pH 3.5 glycine-HCl buffer for 5 min to separate the DJ-1 antibody-antigen immuno-complex. After each regeneration, the electrodes were washed thoroughly and treated again with DJ-1 solution (470 fg mL^{-1}). While the developed sensor gave approximately the same impedimetric response to the concentration of DJ-1 of 470 fg mL^{-1} for 7 cycles, it was observed that the impedimetric signal decreased with the first DJ-1 treatment after the seventh cycle (Fig. 3A).

The high regeneration capacity of the developed neuro-biosensor system in acidic environments can be attributed to the long durability of the multi-walled carbon nanotube. In addition, the compatibility of MWCNT within the hybrid structure allowed the neuro-biosensor system to regenerate the DJ-1 protein over 7 cycles.

Selectivity is crucial because the developed bioreceptor must be capable of detecting a specific analyte (DJ-1) in a sample containing other additives and contaminants. The affinity that the developed neurobiosensor may show against other proteins was observed in the presence of Tau-441, an important biomarker of Alzheimer type dementia, SYN-alpha another important marker of Parkinson type dementia and heat shock protein-70 (HSP-70). The affinity of the biosensing complex to these proteins was monitored in the linear determination range (4.7 fg mL^{-1}–4700 fg mL^{-1}) for DJ-1. Although the contribution of the developed complex to charge transfer resistance is negligible, it was seen that the system shows the highest attraction for SYN-alpha protein (Fig. 2C). This high selectivity of the designed neurobiosensor system is likely to result from the increase in MWCNT used in the structure for bioelectrocatalytic activity. The consistency of the AuNP/11-AUT/MWCNT combined platform resulted in high selectivity.

The neuro-biosensor developed for the determination of DJ-1 was stored for 5 weeks in a dry environment and the storage stability was evaluated by measuring the same concentration of DJ-1 (470 fg mL^{-1}). The sensor system was found to remain completely stable for 5 weeks (Fig. 3B). The high surface free energy of AuNP played a major role in maintaining the bioactivity and stability of the biomolecule (anti-DJ-1) immobilized on the sensing surface. In addition, self-assembling monolayers and carbon nanotubes are highly stable materials; the combination of these advantages in this neuro-biosensor system resulted in the absence of a time-dependent change in the DJ-1 response.

3.4. Real-time monitoring with single frequency impedance

The kinetic behavior of the immunocomplex formed between anti-DJ-1 and DJ-1 was evaluated by monitoring the changes in impedance and phase angle in non-Faradic environment at constant frequency with time. The frequency (5 Hz) to be applied to the system was selected and analyzed using the Bode curve (Fig. 2F, logarithm of the absolute impedance (| Z |) and the phase shift).

Kinetic monitoring of anti-DJ-1 and DJ-1 immunocomplex formation process was followed by frequency-independent, time-dependent SFI. As shown in Fig. 2F, it was determined that the formation of the immunocomplex is completed in around 20 min. At the end of this period, the change in impedance is approximately

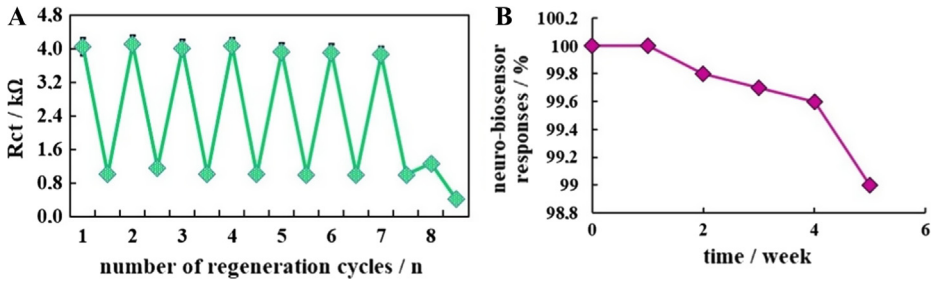

Fig. 3. Regeneration capacity (A) and storage stability (B) of designed neuro-biosensor.

150 Ωs, while the decrease in phase angle is 4.5°. These impedimetric changes support the successful formation of the anti-DJ-1 antibody/DJ-1 biocomplex on the sensing surface.

3.5. Capture of target protein DJ-1 from CSF and saliva samples

The applicability of the developed neuro-biosensor in clinical samples was determined by analyzing DJ-1 protein in cerebrospinal fluid and saliva samples collected randomly among patients who applied to the Neurology Unit of Namık Kemal University Research and Application Hospital. Concentrations of 235 fg mL^{-1} and 3500 fg mL^{-1} of DJ-1 protein were added to CSF and saliva samples by using the standard addition method and EIS analysis was performed with the nanocomposite-doped neuro-biosensor system. The relative standard deviation and recovery analytical values of the measurements were calculated using the calibration graph.

There are studies showing that the mean value of DJ-1 protein in the saliva of men and women who have not been diagnosed with Parkinson's disease is 4 ng/mL [13] and the mean value in CSF is 38 ng/mL [8]. Based on these studies, 10^6-fold dilution was performed in the samples. The results obtained with the standard addition method are shown in Table 2.

The presence of structures such as amylase, lysozyme, immunoglobulin (lgA, lgG, lgM), urea, uric acid in saliva may have caused deviation in biostatistical analyzes. The results from clinical samples show that the ITO-based AuNP/11-AUT/MWCNT-modified disposable neuro-biosensor system showed high sensitivity for evaluation of the target protein DJ-1, even in complex physiological environments. There is no doubt the role of nanomaterials (AuNP-MWCNT) is important in obtaining this sensitivity. In view of these results, it is promising that this disposable neuro-biosensor system, which is easy to use, has low preparation cost, has a high response rate and has remarkable storage stability, is open to potential applications in the clinical field. Moreover, it should be underlined that no technique was reported in the literature for the identification of DJ-1 protein, an important marker of Parkinson-type dementia. In this respect, the suggested method is also noteworthy in terms of contributing to the scientific literature.

3.6. SEM, AFM and FTIR results

During the step-by-step development of the neuro-biosensor system, morphological changes on the surface were monitored by scanning electron microscopy (Fig. 4).

Fig. 4A is a view of the ITO surface after gold nanoparticles were deposited. After deposition of the gold nanoparticles, the monolayer film formed by the amino thiol is as shown in Fig. 4B. In the monolayer, bar deposits are formed in some places. The morphological change in the carbon nanotube on the electrode surface as a result of the covalent interaction of MWCNT on 11-AUT is shown in Fig. 4C. The globular form obtained by the immobilization of anti-DJ-1 on the surface is clearly seen in 5D. In the step

Table 2
Determination of DJ-1 concentrations in CSF and saliva samples with the developed neurobiosensor system.

Saliva number	Content of DJ-1 (c/fg.mL^{-1})	Addition content (c/fg ml^{-1})	Detection content (c/fg ml^{-1}, n = 3)	RSD (%, n = 3)	Recovery (%)
1	1609	235	1850/1915.5/1905.5	2.1	102.2
		3500	5110/5212.2/5111	1.1	100.7
2	5.2	235	238.8/242 /255.5	3.7	102.1
		3500	3550/3542 /3512.5	0.5	100.8
3	4.9	235	242.5 /266.6/301.5	10.9	112.6
		3500	3492.5/3495.5/3406.6	1.4	99
4	5.7	235	242.7/255.9/222.2	7.1	99.8
		3500	3601/3550/3505	1.4	101.4
5	6.2	235	255.3/212.5/223.4	9.6	95.7
		3500	3612.2/3412.9/3511	2.8	100.2
6	223.5	235	466.5/459.5/424	5.1	98.1
		3500	3750/3705.5/3710.6	0.6	100.1
CSF number	Content of DJ-1 (c/fg ml^{-1})	Addition content (c/fg ml^{-1})	Detection content (c/fg ml^{-1}, n=3)	RSD (%, n=3)	Recovery (%)
1	18.5	235	250.5/262.7/260.1	2.5	101.4
		3500	3520/3555/3456.6	1.4	99.8
2	36.5	235	281.5/256.6 /252.4	6.0	97.1
		3500	3540 /3555.5 /3548.8	0.2	100.3
3	15.5	235	250.5/262.4/278.8	5.4	105.6
		3500	3514.4/3502/3571	1.0	104
4	24.4	235	269.9/277.1/264.9	2.3	104.3
		3500	3520/3555/3456.6	0.2	102.3
5	12.7	235	245.5/240.5/238.8	1.4	97.5
		3500	3550/3621/3615.5	1.1	102.4

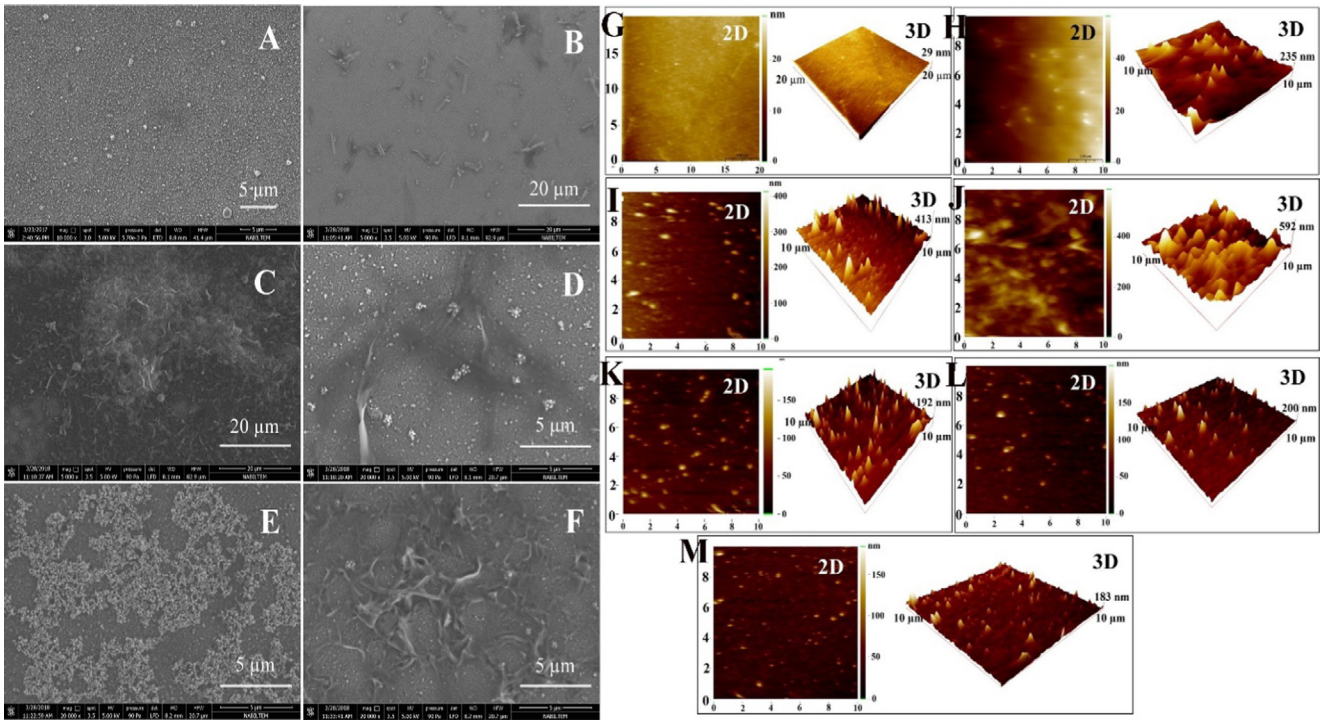

Fig. 4. Step-by-step morphological SEM images for the designed biosensor. (A) ITO-OH/AuNP, (B) ITO/OH/AuNP /11-AUT, (C) ITO/OH/AuNP /11-AUT/MWCNT, (D) ITO/OH/AuNP/11-AUT/MWCNT/anti-DJ-1, (E) ITO/OH/AuNP/11-AUT/MWCNT/anti-DJ-1/BSA, and (F) ITO/OH/AuNP/11-AUT/MWCNT/anti-DJ-1/BSA/DJ-1, AFM results of bare ITO, (G) ITO-OH/AuNP, (H) ITO/OH/AuNP /11-AUT, (I) ITO/OH/AuNP /11-AUT/MWCNT, (J) ITO/OH/AuNP/11-AUT/MWCNT/anti-DJ-1, (K) ITO/OH/AuNP/11-AUT/MWCNT/anti-DJ-1/BSA, and (L) ITO/OH/AuNP/11-AUT/MWCNT/anti-DJ-1/BSA/DJ-1 (M).

where BSA was immobilized on the surface in order to prevent nonspecific adsorption, the morphology of the surface was transformed into shape 5E. The immuno-interaction of DJ-1 with the surface provided a reticulated appearance to the surface morphology as shown in Fig. 4F.

While performing the design steps of the neuro-biosensor, changes in surface morphology were also monitored by AFM. Functionalization of the DJ-1 neuro-biosensor surface caused changes in surface morphology. The almost smooth surface of the plain ITO electrode changes with progressive modifications supported by the results obtained from AFM. When the root mean square (rms) of surface roughness were examined, the bare ITO electrode had a roughness of 2.18 nm, and as a result of modifications with AuNP, 11-AUT and MWCNT, it reached 136.78 nm, 56.84 nm, and 83.52 nm respectively. All these changes on the surface support the formation of the sensing platform for the neuro-biosensor. Anti-DJ-1 immobilization with a decrease in rms value of 17.53 nm indicates that anti-DJ-1 creates a barrier effect on the surface, and then the decrease of DJ-1 to 13.80 nm with immobilization indicates that the barrier effect gradually increases (Fig. 4).

While developing the neuro-biosensor for the determination of DJ-1, the bonds formed were monitored by FTIR. Fig. 4S-A is the spectrum of bonds seen after the SAM layer is formed by 11-AUT. The flat peak at 3270 cm^{-1} is the vibration peak of the free N-H group. The small vibration band of C-H at 2950 cm^{-1} is likely to belong to the aliphatic bond. The weak peak around 2800 cm^{-1} may belong to S-H groups which are in free state. When all these are considered together, the structure points to 11-AUT. The FTIR results obtained after immobilization of Anti-DJ-1 are shown in Fig. 4S-B. The vibration band at 3250 cm^{-1} belongs to the N-H groups likely to be present in the protein structure. The most defined FTIR information about immobilization belongs to the peak at 1645 cm^{-1}. This peak indicates the amide bond between NH_2 and COO groups and supports immobilization of anti-DJ-1 antibody.

4. Conclusion

Early diagnosis of PD will significantly contribute to the course of treatment and change the individual's lifestyle. This neuro-biosensor system, which can selectively detect DJ-1 protein, a potential neurodegeneration biomarker, has the advantages of AuNP-MWCNT nanocomposite. The well-packaged 11-AUT layer on the sensing unit surface guides the electrochemical contact with the compatibility of the nanocomposite. When the developed neuro-biosensor system has the SFI technique applied, it is possible to monitor the antigen antibody immunoreaction. The proposed platform demonstrates high sensitivity and reproducibility by detecting the DJ-1 protein at the femtogram level and over a wide assay range (4.7 fg mL^{-1}–4700 fg mL^{-1}). The high selectivity of the system, even in complex fluid environments such as CSF and saliva, emphasizes that the 11-AUT-modified disposable ITO electrodes with MWCNT-AuNP nanocomposite is a successful sensing platform. Finally, this study is innovative and promising because no studies have been reported so far for the detection of DJ-1 protein.

Declaration of Competing Interest

The authors declare that they have no known competing financial interests or personal relationships that could have appeared to influence the work reported in this paper.

Appendix A. Supplementary material

Supplementary data to this article can be found online at https://doi.org/10.1016/j.bioelechem.2020.107734.

References

[1] S.E. Oh et al., The Parkinson's disease gene product DJ-1 modulates miR-221 to promote neuronal survival against oxidative stress, Redox Biol. 19 (2018) 62–73, https://doi.org/10.1016/j.redox.2018.07.021.

[2] R. Chen et al., Parkinson's disease protein DJ-1 regulates ATP synthase protein components to increase neuronal process outgrowth, Cell Death Dis. 10 (6) (2019) 469, https://doi.org/10.1038/s41419-019-1679-x.

[3] N. Lev et al., Role of DJ-1 in Parkinson's disease, J. Mol. Neurosci. 29 (3) (2006) 215–225, https://doi.org/10.1385/JMN:31:03:307.

[4] Y. Saito, Oxidized DJ-1 as a possible biomarker of Parkinson's disease, J. Clin. Biochem. Nutrit. 54 (3) (2014) 138–144, https://doi.org/10.3164/jcbn.13-108.

[5] C. An et al., Expression of the DJ-1 protein in the serum of Chinese patients with Parkinson's disease, Neurosci. Lett. 665 (2018) 236–239, https://doi.org/10.1016/j.neulet.2017.12.023.

[6] D. Antipova, R. Bandopadhyay, Expression of DJ-1 in neurodegenerative disorders, in: H. Ariga, S. Iguchi-Ariga (Eds.), DJ-1/PARK7 Protein. Advances in Experimental Medicine and Biology, vol. 1037, Springer, Singapore, 2017, https://doi.org/10.1007/978-981-10-6583-5_3.

[7] J. Choi et al., Oxidative damage of DJ-1 is linked to sporadic Parkinson and Alzheimer diseases, J. Biol. Chem. 281 (16) (2006) 10816–10824, https://doi.org/10.1074/jbc.M509079200.

[8] Z. Hong et al., DJ-1 and α-synuclein in human cerebrospinal fluid as biomarkers of Parkinson's disease, Brain 133 (3) (2010) 713–726, https://doi.org/10.1093/brain/awq008.

[9] L. Parnetti et al., Cerebrospinal fluid biomarkers in Parkinson disease, Nat. Rev. Neurol. 9 (3) (2013) 131, https://doi.org/10.1093/brain/awq008.

[10] I. Devic et al., Salivary α-synuclein and DJ-1: potential biomarkers for Parkinson's disease, Brain 134 (7) (2011), https://doi.org/10.1093/brain/awr015 e178.

[11] J.M. Masters et al., Elevated salivary protein in Parkinson's disease and salivary DJ-1 as a potential marker of disease severity, Parkinsonism Related Disord. 21 (10) (2015) 1251–1255, https://doi.org/10.1016/j.parkreldis.2015.07.021.

[12] W. Poewe, et al., Parkinson disease, Nature reviews Disease primers, (2017) 17013 https://doi.org/10.1038/nrdp.2017.13.

[13] W.-Y. Kang et al., Salivary DJ-1 could be an indicator of Parkinson's disease progression, Front. Aging Neurosci. 6 (2014) 102, https://doi.org/10.3389/fnagi.2014.00102.

[14] W. Le et al., Can biomarkers help the early diagnosis of Parkinson's disease?, Neuroscience bulletin 33 (5) (2017) 535–542, https://doi.org/10.1007/s12264-017-0174-6.

[15] L. Parnetti et al., Cerebrospinal fluid lysosomal enzymes and alpha-synuclein in Parkinson's disease, Mov. Disord. 29 (8) (2014) 1019–1027, https://doi.org/10.1002/mds.25772.

[16] C. Marras, A. Lang, Parkinson's disease subtypes: lost in translation?, J. Neurol. Neurosurg. Psychiatry 84 (2013) 409–415, https://doi.org/10.1136/jnnp-2012-303455.

[17] Y. Wu, W. Le, J. Jankovic, Preclinical biomarkers of Parkinson disease, Arch. Neurol. 68 (1) (2011) 22–30, https://doi.org/10.1001/archneurol.2010.321.

[18] N. Saifuddin, A. Raziah, A. Junizah, Carbon nanotubes: a review on structure and their interaction with proteins, J. Chem. 2013 (2012), https://doi.org/10.1155/2013/676815.

[19] C.-M. Tilmaciu, M.C. Morris, Carbon nanotube biosensors, Front. Chem. 3 (2015) 59, https://doi.org/10.3389/fchem.2015.00059.

[20] Z. Wang, Z. Dai, Carbon nanomaterial-based electrochemical biosensors: an overview, Nanoscale 7 (15) (2015) 6420–6431, https://doi.org/10.1039/C5NR00585J.

[21] M. Varna, H.V. Xuan, E. Fort, Gold nanoparticles in cardiovascular imaging, Wiley Interdiscip. Rev. Nanomed. Nanobiotechnol. 10 (1) (2018), https://doi.org/10.1002/wnan.1470.

[22] J. Baniukevic et al., Magnetic gold nanoparticles in SERS-based sandwich immunoassay for antigen detection by well oriented antibodies, Biosens. Bioelectron. 43 (2013) 281–288, https://doi.org/10.1016/j.bios.2012.12.014.

[23] C. Kokkinos, A. Economou, M.I. Prodromidis, Electrochemical immunosensors: critical survey of different architectures and transduction strategies, TrAC, Trends Anal. Chem. 79 (2016) 88–105, https://doi.org/10.1016/j.trac.2015.11.020.

[24] E.B. Bahadır, M.K. Sezgintürk, A review on impedimetric biosensors, Artif. Cells Nanomed. Biotechnol. 44 (1) (2016) 248–262, https://doi.org/10.3109/21691401.2014.942456.

[25] F. Malvano, R. Pilloton, D. Albanese, Label-free impedimetric biosensors for the control of food safety–a review, Int. J. Environ. Anal. Chem. 100 (4) (2020) 468–491, https://doi.org/10.1080/03067319.2019.1667096.

[26] J. Muñoz, R. Montes, M. Baeza, Trends in electrochemical impedance spectroscopy involving nanocomposite transducers: characterization, architecture surface and bio-sensing, TrAC, Trends Anal. Chem. 97 (2017) 201–215, https://doi.org/10.1016/j.trac.2017.08.012.

[27] J.S. Daniels, N. Pourmand, Label-free impedance biosensors: opportunities and challenges, Electroanalysis 19 (12) (2007) 1239–1257, https://doi.org/10.1002/elan.200603855.

[28] M. Grossi, B. Riccò, Electrical impedance spectroscopy (EIS) for biological analysis and food characterization: a review, J. Sens. Sens. Syst. 6 (2017) 303–325, https://doi.org/10.5194/jsss-6-303-2017.

[29] A. Groß et al., The effect of the thickness of the sensitive layer on the performance of the accumulating NOx sensor, Sensors 12 (9) (2012) 12329–12346, https://doi.org/10.3390/s120912329.

[30] K.D. Comeau, M.V. Meli, Effect of alkanethiol chain length on gold nanoparticle monolayers at the air–water interface, Langmuir 28 (1) (2012) 377–381, https://doi.org/10.1021/la202895n.

[31] R. Radhakrishnan et al., Impedance biosensors: Applications to sustainability and remaining technical challenges, ACS Sustainable Chem. Eng. 2 (7) (2014) 1649–1655, https://doi.org/10.1021/sc500106y.

[32] M.N.S. Karaboğa, M.K. Sezgintürk, Cerebrospinal fluid levels of alpha-synuclein measured using a poly-glutamic acid-modified gold nanoparticle-doped disposable neuro-biosensor system, Analyst 144 (2) (2019) 611–621, https://doi.org/10.1039/C8AN01279B.

[33] B. Özcan, M.K. Sezgintürk, Highly sensitive and cost-effective ITO-based immunosensor system modified by 11-CUTMS: analysis of SOX2 protein in real human serum, Int. J. Biol. Macromol. 130 (2019) 245–252, https://doi.org/10.1016/j.ijbiomac.2019.02.112.

[34] Y. Ma et al., Direct electrodeposition of gold nanoparticles on indium tin oxide surface and its application, Biosens. Bioelectron. 24 (5) (2009) 1480–1483, https://doi.org/10.1016/j.bios.2008.10.007.

[35] M.Q. Zhao et al., Flexible MXene/carbon nanotube composite paper with high volumetric capacitance, Adv. Mater. 27 (2) (2015) 339–345, https://doi.org/10.1002/adma.201404140.

[36] S. Bourigua et al., Impedimetric immunosensor based on SWCNT-COOH modified gold microelectrodes for label-free detection of deep venous thrombosis biomarker, Biosens. Bioelectron. 26 (4) (2010) 1278–1282, https://doi.org/10.1016/j.bios.2010.07.004.

[37] M.N.S. Karaboğa, M.K. Sezgintürk, Determination of C-reactive protein by PAMAM decorated ITO based disposable biosensing system: a new immunosensor design from an old molecule, Talanta 186 (2018) 162–168, https://doi.org/10.1016/j.talanta.2018.04.051.

[38] M. Holzinger, A. Le Goff, S. Cosnier, Nanomaterials for biosensing applications: a review, Front. Chem. 2 (2014) 63, https://doi.org/10.3389/fchem.2014.00063.

[39] A. Ramanavicius et al., Electrochemical impedance spectroscopy of polypyrrole based electrochemical immunosensor, Bioelectrochemistry 79 (1) (2010) 11–16, https://doi.org/10.1016/j.bioelechem.2009.09.013.

[40] V. Spampinato et al., Surface analysis of gold nanoparticles functionalized with thiol-modified glucose SAMs for biosensor applications, Front. Chem. 4 (2016) 8, https://doi.org/10.3389/fchem.2016.00008.

[41] E. Pensa et al., The chemistry of the sulfur–gold interface: in search of a unified model, Acc. Chem. Res. 45 (8) (2012) 1183–1192, https://doi.org/10.1021/ar200260p.

[42] S. Campuzano et al., Characterization of alkanethiol-self-assembled monolayers-modified gold electrodes by electrochemical impedance spectroscopy, J. Electroanal. Chem. 586 (1) (2006) 112–121, https://doi.org/10.1016/j.jelechem.2005.09.007.

[43] M.I. Prodromidis, Impedimetric immunosensors—A review, Electrochim. Acta 55 (14) (2010) 4227–4233, https://doi.org/10.1016/j.electacta.2009.01.081.

[44] F. Fasmin, R. Srinivasan, Detection of nonlinearities in electrochemical impedance spectra by Kramers-Kronig Transforms, J. Solid State Electrochem. 19 (6) (2015) 1833–1847, https://doi.org/10.1007/s10008-015-2824-9.